A FAMILY OF SEMI-LAGRANGIAN SCHEMES

Jean Côté*, Sylvie Gravel*, André Méthot#,
Alain Patoine#, Michel Roch* and Andrew Staniforth*
* Recherche en prévision numérique
# Canadian Meteorological Centre
Dorval, CANADA

1. INTRODUCTION

Since Robert et al. (1985) first demonstrated a semi-implicit semi-Lagrangian discretization of the hydrostatic primitive equations, this method has found increasing favour at weather-forecasting and climate centres throughout the world (e.g., Bates et al. 1993; McDonald and Haugen 1992; Purser and Leslie 1994; Ritchie and Beaudoin 1994; Ritchie et al. 1995; Tanguay et al. 1989; Williamson and Olson 1994).

Although it has been known for some time (Kaas 1987; Coiffier et al. 1987; Staniforth & Côté 1991; Tanguay et al. 1992) that semi-implicit semi-Lagrangian schemes can experience difficulties at high Courant number in the presence of orography, it is only recently that this problem has been elucidated. In Rivest et al. (1994), hereafter referred to as RSR94, its source was clearly identified and a solution proposed in a two-time-level context. It consists of off-centering the semi-implicitly-treated terms along the trajectory, and Rivest & Staniforth (1995) have proposed a possible retrofit scheme for three-time-level-based centered schemes. Héreil & Laprise (1995) have recently extended the RSR94 analysis to the semi-implicit semi-Lagrangian discretization of Tanguay et al. (1990) of the non-hydrostatic Euler equations.

Two questions emerge naturally from the RSR94 study. First, is it possible to exploit the decentering of the time scheme to create a richer family of semi-Lagrangian time schemes that not only address the orographic resonance problem, but also have other interesting properties: e.g. enhanced accuracy or simplicity. The response to the first part of this question is straightforward. It is indeed possible to create a richer family, and it remains only to determine its properties. It turns out that one member of this generalized family is equivalent to the $O(\Delta t^3)$ scheme proposed in McDonald (1987). This then leads to the second question, that posed in McDonald (1987): "*It would be interesting to test this scheme in a realistic setting to see if the promise of high accuracy in both Δt and Δx held up in practice*".

The goals of the present paper are: to present this generalized family of schemes; to assess the merits of different members of this family based on both theory and practice and to thereby answer McDonald (1987)'s question; and to present some results obtained using the original Rivest et al. (1994) semi-implicit semi-Lagrangian scheme in a prototype of a global variable-resolution baroclinic model currently under development.

The generalized family of time schemes is defined in Section 2, and its resonance and stability properties analysed therein. A first practical assessment is accomplished by integrating a global shallow-water model subject to orographic forcing for various members of the family of schemes examined theoretically in the previous section. These results are presented in Section 3. A brief description of the global variable-resolution baroclinic prototype is given in Section 4, and results from it are presented in Section 5. These latter tests are performed in the absence of orography. Finally, some conclusions are summarized in Section 6.

2. THEORY

2.1 The generalized family of $O(\Delta t^2)$ schemes

The linearized one-dimensional shallow-water equations after a three-time-level semi-implicit semi-Lagrangian discretization may be written as (cf. RSR94):

$$\frac{Dv}{Dt} + \overline{fu}^t = 0, \tag{2.1}$$

$$\frac{Du}{Dt} + \overline{\frac{\partial \phi}{\partial x} - fv}^t = -\overline{\frac{\partial \phi_s}{\partial x}}^t, \tag{2.2}$$

$$\frac{D\phi}{Dt} + \Phi \overline{\frac{\partial u}{\partial x}}^t = 0, \tag{2.3}$$

where ϕ and ϕ_s are respectively the fluid depth and orographic height multiplied by g, the other symbols have their usual meaning, and for the *generalized family* of schemes introduced here:

$$\frac{DF}{Dt} = \frac{1}{\Delta t}\left[(1+\varepsilon)F^n - (1+2\varepsilon)F^{n-1} + \varepsilon F^{n-2}\right], \tag{2.4}$$

$$\overline{F}^t = \frac{(1+\delta+\varepsilon)}{2}F^n + \frac{(1-2\delta)}{2}F^{n-1} + \frac{(\delta-\varepsilon)}{2}F^{n-2}, \tag{2.5}$$

$$F^{n-r} \equiv F\left[x(t) - rU\Delta t, t - r\Delta t\right], \tag{2.6}$$

where $t = n\Delta t$, and r and n are integers.

The basic-state quantities U and Φ are assumed non-zero, and the orographic geopotential ϕ_s is both non-zero and time invariant. The linearized equations before discretization may be recovered by redefining DF/Dt and $\overline{F}^t$ as:

$$\left(\frac{DF}{Dt}\right)_{exact} = \frac{\partial F}{\partial t} + U\frac{\partial F}{\partial x}, \tag{2.7}$$

$$\left(\overline{F}^t\right)_{exact} = F. \tag{2.8}$$

It is possible to rewrite the governing equations (2.1)-(2.3) in terms of the geopotential *height* ($\eta \equiv \phi + \phi_s$) of the fluid's surface instead of its geopotential *thickness* ϕ, as advocated by Ritchie and Tanguay (see their paper in this volume). Note that the essential difference between their approach and the RSR94 one is that the governing equations are rewritten in the following alternate way before discretization:

$$\frac{Dv}{Dt} + \overline{fu}^t = 0, \tag{2.1'}$$

$$\frac{Du}{Dt} + \overline{\frac{\partial \eta}{\partial x} - fv}^t = 0, \tag{2.2'}$$

$$\frac{D\eta}{Dt} + \overline{\Phi\frac{\partial u}{\partial x}}^t = U\overline{\frac{\partial \phi_s}{\partial x}}^t. \tag{2.3'}$$

The change of variable has the effect of slightly changing the way in which the forcing appears in the equations, but it does not change *the form of the unforced terms*, all of which appear on the left-hand sides of the equations. Because of this latter fact, it turns out that the analysis given below of (2.1)-(2.3), and the conclusions drawn therefrom, also apply mutatis mutandis to the system (2.1')-(2.3'). The semi-implicit semi-Lagrangian formulation introduced by Ritchie and Tanguay can therefore be generalized in exactly the same way as that introduced above for the Rivest et al. (1994) one, and this makes the link between the present work and theirs.

The above 2-parameter (δ, ε) family of schemes is the most general $O(\Delta t^2)$-accurate scheme based on three time levels, and is a generalization of the 1-parameter (δ) family presented in RSR94. The parameter δ here is exactly as in RSR94. It was introduced there to decenter the 2-time-level Crank-Nicolson semi-implicit semi-Lagrangian discretization, and thereby address the problem of spurious

orogrophically-induced resonance by introducing a third time level to evaluate the time-averaged contributions along the trajectory. A further new parameter ε has been added here. It optionally introduces the use of a third time level in the evaluation of the time derivatives along the trajectory. This additional degree of freedom might be expected a priori to permit an improvement to the RSR94 family of schemes by reducing the time truncation errors [possibly to $O(\Delta t^3)$] while still maintaining stability and avoiding spurious resonance. Note that McDonald (1987)'s proposed $O(\Delta t^3)$ scheme (cf. his eq.27) is a special case of the generalized family. This is discussed further later. Special cases of the above generalized scheme for particular values of δ and ε are summarized in Table 1.

δ	ε	Scheme
0	0	Crank-Nicolson using time levels t and t-Δt
$\frac{1}{2}$	$-\frac{1}{2}$	Crank-Nicolson using time levels t and t-$2\Delta t$
δ	0	General RSR94 1-parameter (δ) scheme
$\frac{1}{2}$	0	Particular RSR94 scheme, for which results were shown
$\frac{1}{2}$	$\frac{1}{2}$	Backward implicit
$-\frac{1}{6}$	$\frac{1}{6}$	McDonald's proposed $O\left(\Delta t^3\right)$ scheme

Table 1: Particular cases of the generalized scheme as a function of δ and ε.

2.2 Decomposition of the solution of the linearized equations

The complete solution to the linear system (2.1)-(2.3) can be written as the sum of free and forced modes:

$$\begin{bmatrix} v(x,t) \\ u(x,t) \\ \phi(x,t) \end{bmatrix} = \begin{bmatrix} v^{free}(x,t) \\ u^{free}(x,t) \\ \phi^{free}(x,t) \end{bmatrix} + \begin{bmatrix} v^{forced}(x) \\ u^{forced}(x) \\ \phi^{forced}(x) \end{bmatrix}. \tag{2.7}$$

The *free* solutions satisfy (2.1)-(2.3) with the forcing $\phi_s(x)$ set identically to zero. Letting

$$\begin{bmatrix} v^{free}(x,t) \\ u^{free}(x,t) \\ \phi^{free}(x,t) \end{bmatrix} = \begin{bmatrix} v_k^{free} \\ u_k^{free} \\ \phi_k^{free} \end{bmatrix} e^{i(kx+\omega t)}, \tag{2.8}$$

each free mode (there are three for each wavenumber) then satisfies

$$\mathbf{A}(\omega)\begin{bmatrix} v_k^{free} \\ u_k^{free} \\ \phi_k^{free} \end{bmatrix} = 0, \tag{2.9}$$

where

$$\mathbf{A}(\omega) = \begin{bmatrix} \Omega(\omega) & f\Gamma(\omega) & 0 \\ -f\Gamma(\omega) & \Omega(\omega) & ik\Gamma(\omega) \\ 0 & ik\Phi\Gamma(\omega) & \Omega(\omega) \end{bmatrix}, \tag{2.10}$$

$$\Omega(\omega) = \frac{(1+\varepsilon)E^2 - (1+2\varepsilon)E + \varepsilon}{\Delta t} = \frac{[(1+\varepsilon)E - \varepsilon][E-1]}{\Delta t}, \tag{2.11}$$

$$\Gamma(\omega) = \frac{1}{2}\left[(1+\delta+\varepsilon)E^2 + (1-2\delta)E + (\delta-\varepsilon)\right], \tag{2.12}$$

$$E(\omega) = \exp[i(\omega + kU)\Delta t], \tag{2.13}$$

and exact interpolation has been assumed. Setting

$$\det[\mathbf{A}(\omega)] = 0, \tag{2.14}$$

then gives the dispersion relation for ω. Note that for the exact solution of the linearized equations (with no discretization), (2.11)-(2.12) may be replaced by the definitions

$$\Omega_{exact}(\omega) = i(\omega + kU), \tag{2.15}$$

$$\Gamma_{exact}(\omega) = 1, \tag{2.16}$$

and the usual (free) Rossby and gravity-wave dispersion relations then result from (2.14):

$$\begin{aligned} \omega_{exact} &= -kU, && (Rossby), \\ &= -kU \pm k\sqrt{\Phi + \left(\frac{f^2}{k^2}\right)}, && (gravity). \end{aligned} \tag{2.17}$$

The *forced* (steady-state) solutions satisfy (2.1)-(2.3) in the absence of any time variation ($\partial/\partial t \equiv 0$), and may be Fourier decomposed as

$$\begin{bmatrix} v^{forced}(x) \\ u^{forced}(x) \\ \phi^{forced}(x) \end{bmatrix} = \begin{bmatrix} v_k^{forced} \\ u_k^{forced} \\ \phi_k^{forced} \end{bmatrix} e^{ikx}. \tag{2.18}$$

They then satisfy

$$\mathbf{A}(\omega \equiv 0) \begin{bmatrix} v_k^{forced} \\ u_k^{forced} \\ \phi_k^{forced} \end{bmatrix} = \begin{bmatrix} 0 \\ -ik\phi_s \\ 0 \end{bmatrix}. \tag{2.19}$$

Note that for the *exact* solution of the linearized equations (with no discretization), $\mathbf{A}(\omega \equiv 0)$ simplifies to

$$\mathbf{A}_{exact}(\omega \equiv 0) = \begin{bmatrix} ikU & f & 0 \\ -f & ikU & ik \\ 0 & ik\Phi & ikU \end{bmatrix}, \tag{2.20}$$

(cf. RSR94). Physical resonance then occurs when the determinant of $\mathbf{A}_{exact}(\omega \equiv 0)$ vanishes, i.e. when

$$U = \sqrt{\Phi + \left(\frac{f^2}{k^2}\right)}, \tag{2.21}$$

which, as discussed in RSR94, corresponds to supersonic flow and is unlikely to occur in a shallow-water model representative of the atmosphere at 500 hPa.

The existence or not of computational resonance is determined from (2.19), and a scheme's stability from the solutions of the dispersion relation (2.14). Note that the matrix $\mathbf{A}$ defined by (2.10) plays a determining role for both resonance and stability. These latter are respectively discussed in the following two sub-sections. Note also that the elements of $\mathbf{A}$ are independent of whether the equations are written as (2.1)-(2.3) or as (2.1')-(2.3'). This means that the following analysis and its conclusions also apply to the generalization of the Ritchie and Tanguay formulation given in this volume.

2.3 Analysis of computational resonance

For the discretized linear equations, whenever

$$\det[\mathbf{A}(\omega \equiv 0)] = 0, \tag{2.22}$$

the stationary forced gravity modes determined by (2.19) are resonant, and these resonances may be spurious (RSR94). This leads to the following two quadratic equations that govern the resonance of the stationary forced gravity solutions:

$$\left[(1+\varepsilon) \pm i\Lambda\Delta t\frac{(1+\delta+\varepsilon)}{2}\right]E_{res}^2 - \left[(1+2\varepsilon)\,\mathrm{m}\,i\Lambda\Delta t\frac{(1-2\delta)}{2}\right]E_{res} + \varepsilon \pm i\Lambda\Delta t\frac{(\delta-\varepsilon)}{2} = 0, \tag{2.23}$$

where

$$E_{res} \equiv E(\omega \equiv 0) = \exp[ikU\Delta t], \tag{2.24}$$

$$\Lambda^2 = k^2\Phi + f^2. \tag{2.25}$$

Since $kU\Delta t$ is real by definition, resonance is only possible if E_{res} lies on the unit circle, i.e. if

$$|E_{res}| \equiv |E(\omega \equiv 0)| = 1. \tag{2.26}$$

For the special case $\varepsilon = 0$, the conditions (2.23) for resonance in the present 2-parameter (δ, ε) family of schemes reduce to (15) of RSR94 for their 1-parameter (δ) family. The further special case $\delta = \varepsilon = 0$ (cf. Table 1), corresponds to the conditions (9) of RSR94 for the spurious resonance of centered 2-time-level semi-implicit semi-Lagrangian schemes. As discussed in RSR94, spurious resonance occurs for certain combinations of large Courant number and nondimensional wavenumbers of the orographic forcing, and can be avoided by suitably off-centering the time discretization along the trajectory. In the present study this is controlled by the δ and ε parameters.

Summarizing, any of the schemes considered here will be non-resonant provided $|E(\omega \equiv 0)| \neq 1$. They may not however necessarily be stable, and this aspect of the discretization is now examined.

2.4 Analysis of stability

Stability is determined from the dispersion relation obtained by solving (2.14). Thus

$$\left[(1+\varepsilon) + iW\Delta t\frac{(1+\delta+\varepsilon)}{2}\right]E^2 - \left[(1+2\varepsilon) - iW\Delta t\frac{(1-2\delta)}{2}\right]E + \varepsilon + iW\Delta t\frac{(\delta-\varepsilon)}{2} = 0, \quad (2.27)$$

where

$$W = 0, \qquad (Rossby), \quad (2.28)$$

$$= \pm\Lambda = \pm\sqrt{k^2\Phi + f^2}, \quad (gravity), \quad (2.29)$$

and the scheme is stable provided

$$|E| \equiv \left|\exp\left[i(\omega + kU)\Delta t\right]\right| \leq 1. \quad (2.30)$$

Note that (2.27) can be identified with the dispersion relation that would result from applying the generalized family of schemes of the present study to an oscillation equation, yielding the discretization

$$\frac{DF}{Dt} + \overline{iWF}^t = 0, \quad (2.31)$$

where W is real. This is equivalent to having performed a decomposition in terms of the eigen-functions of the matrix $\mathbf{A}$. The leading-order term of the truncation error (obtained in the usual manner via a Taylor-series expansion and placed on the right-hand side of 2.31) is

$$Truncation\ error = iW\left(\frac{1}{12}+\frac{\delta}{2}\right)\left(\Delta t^2\right)\frac{D^2F}{Dt^2}+O\left(\Delta t^3\right). \tag{2.32}$$

For the quadratic associated with the Rossby modes (for which $W=0$), (2.27) factors easily and $E=1$ or $\varepsilon/(1+\varepsilon)$. The first root corresponds to the physical Rossby mode and it is stable since it satisfies (2.30). The other root corresponds to a computational Rossby mode (introduced by discretizing a 1st-order-in-time equation over three time levels), and it will satisfy (2.30) and be stable provided $\varepsilon \geq -1/2$. Now $\varepsilon=-1/2$ corresponds to a centered three-time-level discretization, and this value for ε must be excluded since (see above and RSR94) the stationary forced gravity modes would suffer from spurious resonance. Although satisfaction of the strict inequality $\varepsilon > -1/2$ is sufficient to stabilize the computational Rossby mode, ε should be positive, otherwise it will have the undesirable property of changing the sign of this computational mode at alternate timesteps (timestep decoupling). ε should not only be positive but small to ensure adequate damping of this computational mode during the integration.

For the quadratic associated with the gravity modes (for which $W=\pm\sqrt{k^2\Phi+f^2}$), (2.27) does not factor easily. It is nevertheless possible to get some insight into the influence of δ and ε on the stability of the free gravity solutions by solving (2.27) asymptotically for E for the physical mode when $W\Delta t$ is small. A straightforward but lengthy expansion in terms of $W\Delta t$ for the physical root of (2.27) then yields the following expansion for its modulus:

$$|E|^2 = 1-\delta(1+2\varepsilon)(W\Delta t)^4+\frac{1}{2}\delta(1+2\varepsilon)[1+10\delta+2\varepsilon(1+\varepsilon)](W\Delta t)^6+O\left[(W\Delta t)^8\right]. \tag{2.33}$$

From above, since $(1+2\varepsilon)>0$ for stability of the computational Rossby solution, it is necessary to take

$$\delta > 0, \tag{2.34}$$

in order to both satisfy the stability condition (2.30) and to also remain off resonance. This is a necessary condition for stability. From (2.32), it has the further consequence that the only $O(\Delta t^3)$-accurate member of the present generalized family of three-time-level schemes (i.e. $\delta=-1/6$) is unstable and therefore inadmissible. This is unfortunate. By numerically solving (2.27) when $W=\pm\sqrt{k^2\Phi+f^2}$ for a broad range of values of the parameters $W\Delta t$, δ, and ε, it is found that the valid domain for remaining both stable and off resonance is

$$\delta > 0, \quad \varepsilon > -\frac{1}{2}, \tag{2.35}$$

as suggested by the above analysis.

A corollary of the present analysis is that it addresses the query, first raised in McDonald (1987) and discussed in the above introduction, concerning the viability of the $O(\Delta t^3)$-accurate scheme (cf. his eq. 27) tentatively proposed therein. This scheme corresponds to $(\delta,\varepsilon)=(-1/6,1/6)$ in the present notation, and it is therefore *unstable for gravity modes* since it violates the above-derived condition (2.34).

Summarizing, it is advisable to choose δ and ε from the more restricted domain

$$\delta > 0, \quad \varepsilon \geq 0, \tag{2.36}$$

to avoid having a time-decoupled computational Rossby mode. It is also advisable to use the smallest-possible values of δ and ε (consistent with being adequately off-resonance), to respectively minimize the truncation errors (see 2.32) and to maximally damp the computational Rossby mode of amplitude $\varepsilon/(1+\varepsilon)$.

3. RESULTS USING A SHALLOW-WATER MODEL

3.1 **Preliminaries and control integration ($\delta=\varepsilon=0$)**

The variable-resolution global shallow-water model described in Côté et al. (1993) has been modified to include the present generalized family of semi-implicit semi-Lagrangian time schemes. To evaluate the proposed family of schemes and to provide some guidance on the choice of the values for the parameters δ and ε, the methodology introduced in RSR94 is adopted. The grid configuration and the model orography used here are as depicted in their Figs. 4 and 5. The grid has a uniform ($1/2^\circ$) resolution window over N. America, and the orography is zero everywhere outside this window. The experiments consist of 48-h forecasts initiated from the 500-hPa height and wind analyses of 1200 UTC 12 February 1979 after an implicit-normal-mode initialization. The initialized geopotential used in all of the described experiments is displayed in Fig. 6 of RSR94.

Two methods for computing trajectories were described in RSR94, and for both of these the upstream point at time $t-\Delta t$ is obtained as in Côté et al. (1993) using winds extrapolated forward from those at times $t-\Delta t$ and $t-2\Delta t$ to $t-(\Delta t/2)$. In the first of the two methods the upstream point at time $t-2\Delta t$ is obtained by simply extending backward the great-circle trajectory that joins the arrival point at time t to the already-determined upstream point at time $t-\Delta t$ by a distance equal to that between them. In the second method, the trajectory between the arrival point at time t and the upstream point at time $t-2\Delta t$ is determined in the same way as for the trajectory between the arrival point at time t and the $t-\Delta t$ upstream point, except that the wind field at time $t-\Delta t$ is used and the time interval is twice as large. This gives rise to a piecewise-defined trajectory rather than the continuous great-circle one of the first method. For the results shown in RSR94, the trajectories were computed using the first method. This was

done on the basis that the results using either of the two methods were very similar, with a small advantage for the second method, but the first method was a little cheaper computationally. However it was found in the present study that the use of the first method significantly degrades the results for some of the other members of the generalized family of schemes. Therefore the trajectories for all of the integrations presented here that require evaluation at the $t-2\Delta t$ upstream point were computed using the piecewise-defined trajectories of the second method.

Figure 1 shows the "control" 48-h forecast of the total geopotential height $[(\phi+\phi_s)/g]$ obtained using the standard two-time-level semi-implicit semi-Lagrangian scheme ($\delta=\varepsilon=0$) with a timestep of 10 min and is identical to Fig. 7 of RSR94. No spurious noise is apparent in the vicinity of the Rockies because of the small (significantly less than unity) Courant number. This integration serves as the standard of comparison in what follows. Integrations at large Courant number (with Δt = 60 min) for various members of the generalized family are compared against it below. Note that for a timestep this large, the standard two-time-level scheme manifests spurious resonance (see Fig. 8 of RSR94).

3.2 An $O(\Delta t^2)$-accurate backward-implicit scheme ($\delta=1/2, \varepsilon=1/2$)

The solution proposed in RSR94 to address the spurious-resonance problem of the standard two-time-level scheme at large Courant number is to decenter the scheme. This is done by adding a third time level in the evaluation of terms that are averaged along the trajectory (and changing the averaging weights), while leaving the semi-Lagrangian discretization of the total derivatives unchanged. It corresponds to evaluating the total derivatives in the simplest, most compact, fashion at the expense of complicating the evaluation of the other terms. The alternative examined in this sub-section is to do the contrary, viz. to maximally simplify the computation of the other terms by evaluating them entirely at the arrival point with weight one, and to decenter the evaluation of the total derivatives by adding a third time level and changing the weights appropriately. This corresponds to setting $\delta=1/2, \varepsilon=1/2$ in the present generalized family (we label this scheme *backward-implicit*) rather than choosing $\delta=1/2, \varepsilon=0$ as used to produce the results shown in RSR94. It has the advantage of no longer computing terms such as $\nabla\phi$ and $\nabla\cdot V$ at times $t-\Delta t$ and $t-2\Delta t$ since they are not needed. Both of these schemes have the same value of δ, and both are formally $O(\Delta t^2)$-accurate with the same coefficient for the leading-order error term (cf. 2.32 with δ set to 1/2).

Figure 2 displays the 48-h forecast for the described backward-implicit scheme using a 60-min timestep. Comparing it to the control (Fig. 1) and the corresponding result shown in RSR94 using the same timestep (their Fig. 11), it is seen that this backward-implicit scheme at this timestep is about as effective in addressing the spurious resonance problem as is the RSR94 scheme (with δ set to 1/2).

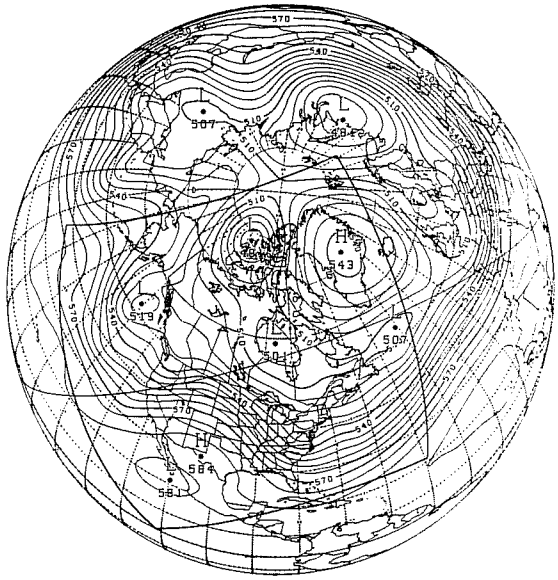

Fig. 1 The geopotential height (dam) for the 48-h "control" forecast using a centered 2-time-level scheme $(\delta = \varepsilon = 0)$ with Δt =10 min.

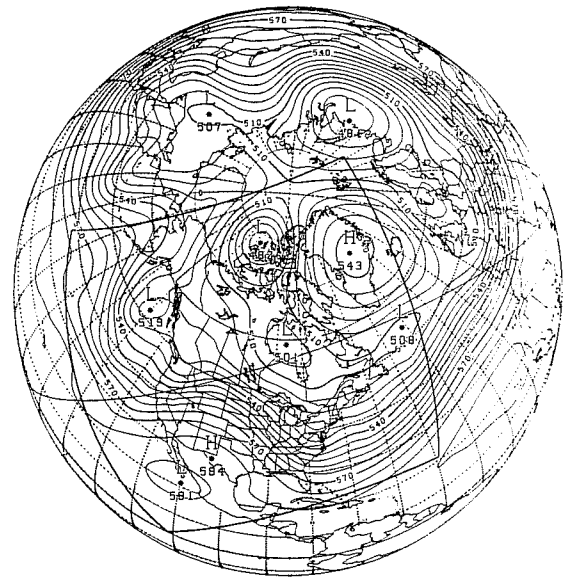

Fig. 2 As in Fig. 1, but for the $O(\Delta t^2)$ "backward-implicit" scheme $(\delta = 1/2, \varepsilon = 1/2)$ with Δt = 60 min.

Fig. 3 As in Fig. 1, but for an uncentered RSR94 scheme $(\delta = 1/6, \varepsilon = 0)$ with Δt = 60 min.

3.3 Another member of the RSR94 family of schemes ($\delta = 1/6, \varepsilon = 0$)

In RSR94, results were only shown for one specific value of the free parameter of their family of schemes, viz. $\delta = 1/2$. It was argued that this was a good (but not necessarily optimal) choice. A careful examination of Fig. 3 of RSR94, where the ratio of the amplitudes of the numerical and analytical geopotentials is displayed, suggests that it may be possible to use a value as small as $\delta = 1/6$ and still remain acceptably far removed from resonance or near-resonance. Figure 3 displays the 48-h forecast for this scheme ($\delta = 1/6, \varepsilon = 0$). It is seen that while the forecast is quite close to the corresponding result with $\delta = 1/2, \varepsilon = 0$ (Fig. 11 of RSR94), it is nevertheless a little more noisy over the Rockies. This indicates that for this choice of orography and timestep, the optimal value of δ lies somewhere between 1/6 and 1/2. If δ is chosen to be smaller than 1/6 then spurious resonance will manifest itself, and if it is taken to be greater than 1/2, then the time truncation error (see 2.32) will increase.

3.4 Further experiments

A set of further 48-h forecasts has been performed, with timesteps varying from 30 min to 120 min, using a variety of values for δ and ε. The specific parameter values used were (δ,ε)= (1/2,0), (1/2,1/2), (1/6,0) and (1/8,1/8). These schemes respectively correspond to: the RSR94 ($\delta = 1/2$), backward-implicit, and RSR94 ($\delta = 1/6$) schemes; and a scheme in the new family lying somewhere between the RSR94 ($\delta = 1/2$) and backward-implicit extremes. The rms geopotential height differences between these forecasts and that of the control one (Fig. 1) have been computed and are displayed in Fig. 4.

It is seen that all of these schemes behave similarly for timesteps as long as one hour, and all are very close to the control forecast with rms differences wrt the control of less than 1.7 m. This is considerably smaller than the criterion of 4m used in RSR94 to determine acceptability. For larger timesteps the rms differences wrt the control for each of the forecasts, except one, behave very similarly and meet the 4 m criterion for timesteps as long as 100 min. The exception is the backward-implicit scheme ($\delta = \varepsilon = 1/2$) for which the difference growth is somewhat faster, and the maximum timestep that satisfies the 4m criterion is reduced to approximately 85 min. Although it is a viable scheme, it is not as good as the others considered for very large timesteps, e.g. the rms difference wrt the control with a 120 min timestep is almost twice that of the others. At first glance this is surprising since the leading-order truncation error (cf. 2.32) of the backward-implicit scheme is exactly the same as that of the RSR94 scheme with (δ,ε)= (1/2,0). However this behaviour can be explained by the fact that the leading-order term for the damping rate (see 2.33) depends on ε and is twice as large in the backward-implicit scheme than in the RSR94 ($\delta = 1/2$) one.

4. A GLOBAL VARIABLE-RESOLUTION BAROCLINIC MODEL

A two-dimensional prototype (Côté et al. 1993) of a global variable-resolution model has been developed to provide the "proof-of-concept" for the horizontal variable-resolution strategy, and it has been tested extensively on a variety of meshes. The formulation has been generalized to three dimensions and dry

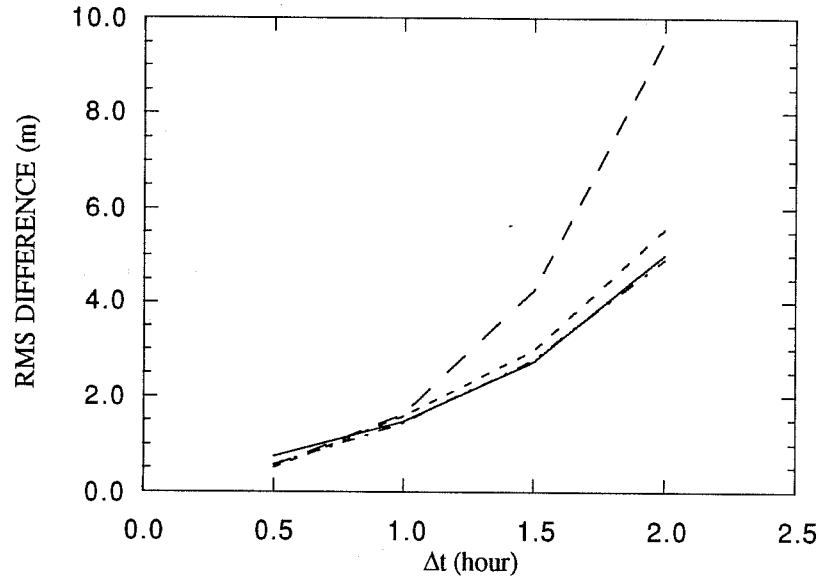

Fig. 4 The rms geopotential height differences (m) of four schemes wrt the control as a function of timestep (h). Solid - RSR94 $(\delta = 1/2, \varepsilon = 0)$; dash/dot - RSR94 $(\delta = 1/6, \varepsilon = 0)$; long dashed - backward implicit $(\delta = 1/2, \varepsilon = 1/2)$; short dashed - $(\delta = 1/8, \varepsilon = 1/8)$.

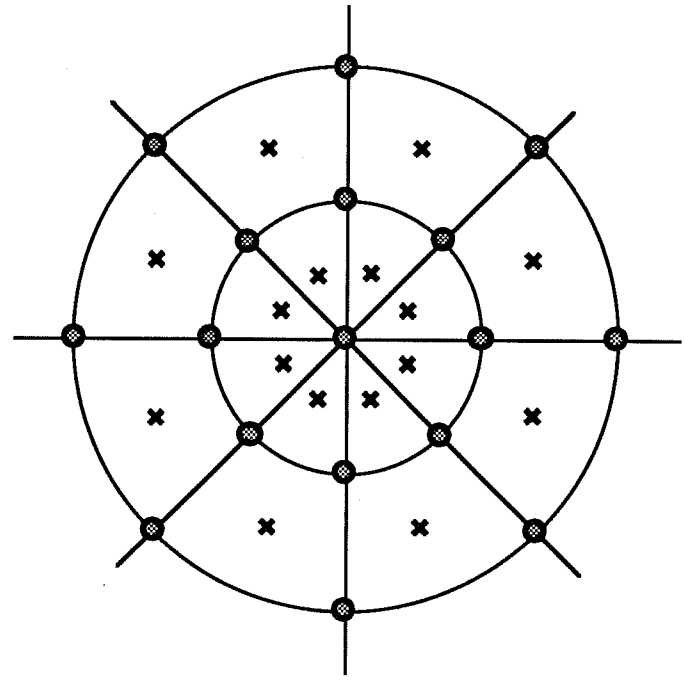

Fig. 5 Schematic for horizontal placement of variables, displayed around a pole. Circled points: p, ϕ. Crossed points: $\mathbf{V}$, T, η.

hydrostatic primitive-equations prototype is currently undergoing testing, validation and refinement. Some preliminary results were given in Côté et al. 1995, and some further results are presented in Section 5 of the present paper. The coding of a moist version is almost complete.

4.1 Governing equations

The equations are those that govern the flow of a frictionless adiabatic hydrostatic fluid on a rotating sphere. A terrain-following hybrid coordinate is defined as

$$\eta = \frac{p - p_T}{p_S - p_T} = \frac{p^* - p_T^*}{p_S^* - p_T^*}, \tag{4.1}$$

where

$$p^* = p_T^* + \left(p_S^* - p_T^*\right)\eta, \tag{4.2}$$

p_S and p_T are the respective pressures at the bottom and top of the atmosphere, and p_S^* and $p_T^* \equiv p_T$ are the respective bottom and top constant pressures of a motionless isothermal ($T^* \equiv$ constant) reference atmosphere. Equation (4.2) is a direct consequence of the definition (4.1) of the vertical coordinate, and permits the thermodynamic equation to be written in such a way as to ensure the computational stability of the gravitational oscillations. The governing equations in this coordinate system then become:

$$\frac{d\mathbf{V}^H}{dt} + RT\nabla \ln p + \nabla\phi + f\left(\mathbf{k}\times\mathbf{V}^H\right) = 0, \tag{4.3}$$

$$\frac{d}{dt}\ln\left|\frac{\partial p}{\partial \eta}\right| + \nabla\cdot\mathbf{V}^H + \frac{\partial \dot{\eta}}{\partial \eta} = 0, \tag{4.4}$$

$$\frac{d}{dt}\left[\ln\left(\frac{T}{T^*}\right) - \kappa \ln\left(\frac{p}{p^*}\right)\right] - \kappa\dot{\eta}\frac{d}{d\eta}\left(\ln p^*\right) = 0, \tag{4.5}$$

$$\frac{\partial\phi}{\partial\eta} = -RT\frac{\partial \ln p}{\partial\eta}, \tag{4.6}$$

where

$$\frac{d}{dt} = \frac{\partial}{\partial t} + \mathbf{V}^H\cdot\nabla + \dot{\eta}\frac{\partial}{\partial\eta}, \tag{4.7}$$

$\phi = gz$ is the geopotential height, and $\kappa = R/c_p$. In the above, eqns (4.3)-(4.6) are respectively the horizontal momentum, continuity, thermodynamic and hydrostatic equations.

The boundary conditions are periodicity in the horizontal; and no motion across the top and bottom of the atmosphere, where the top is at constant pressure p_T. Thus

$$\dot{\eta} \equiv \frac{d\eta}{dt} = 0 \text{ at } \eta = 0,1. \tag{4.8}$$

4.2 Temporal discretization

The time discretization is fully-implicit/ semi-Lagrangian. Consider a prognostic equation of the form

$$\frac{dF}{dt} + G = 0, \tag{4.9}$$

where F represents one of the prognostic quantities $\{\mathbf{V}^H,\ \ln|\partial p/\partial\eta|,\ \ln(T/T^*) - \kappa\ln(p/p^*)\}$, and G represents the remaining terms, some of which are nonlinear. Such an equation is approximated by time differences and weighted averages along a trajectory determined by an approximate solution to

$$\frac{d\mathbf{x}_3}{dt} = \mathbf{V}_3(\mathbf{x}_3, t), \tag{4.10}$$

where $\mathbf{x}_3$ and $\mathbf{V}_3$ are the three-dimensional position and velocity vectors respectively. Thus

$$\frac{\left(F^n - F^{n-1}\right)}{\Delta t} + \left(\frac{3}{4}G^n + \frac{1}{4}G^{n-2}\right) = 0, \tag{4.11}$$

where $\psi^n = \psi(\mathbf{x}_3, t)$, $\psi^{n-m} = \psi[\mathbf{x}_3(t - m\Delta t), t - m\Delta t]$, $\psi = \{F, G\}$, $t = n\Delta t$.

Note that this scheme is decentered along the trajectory as in Rivest et al. (1994), in anticipation of the introduction of orography (not included in the results of the present paper). In this way the spurious resonant response arising from a centered approximation in the presence of orography will be avoided. This decentered scheme nevertheless shares the $O(\Delta t^2)$ accuracy of the more usual centered schemes. It corresponds to setting the parameters of the generalized family of schemes to be $(\delta, \varepsilon) = (1/2, 0)$. Cubic interpolation is used everywhere for upstream evaluations (cf. eqn 4.11) except for the trajectory computations (cf. eqn 4.10), where linear interpolation is used with no visible degradation in the results.

Grouping terms at the new time on the left-hand side and known quantities on the right-hand side, eqn (4.11) may be rewritten as

$$\left(F+\frac{3}{4}\Delta tG\right)^n = F^{n-1}-\frac{1}{4}\Delta tG^{n-2}. \tag{4.12}$$

This yields a set of coupled nonlinear equations for the unknown quantities at the meshpoints of a regular grid at the new time t, the efficient solution of which is discussed below. A fully-implicit time treatment, such as that adopted here, of the nonlinear terms has the useful property of being inherently computationally more stable than a more explicit one (e.g. those of Bates et al. 1993 and McDonald and Haugen 1992, whose computational stability is analysed in Gravel et al. 1993).

4.3 Spatial discretisation

A variable-resolution finite-element discretisation, based on that described in Côté et al. (1993), is used in the horizontal with a placement of variables as shown schematically in Fig. 5. It has the advantage that only one set of trajectories is required, although other placements are possible and are being examined. In particular, a cell-integrated version of the model using a C-grid has been coded. The vertical discretisation is modeled after that of Tanguay et al. (1989).

4.4 Solving the coupled nonlinear set of discretized equations

After spatial discretisation the coupled set of nonlinear equations still has the form of eqn (4.12). Terms on the right-hand side, which involve upstream interpolation, are evaluated once and for all. The coupled set is rewritten as a linear one (where the coefficients depend on the basic state) plus a perturbation which is placed on the right-hand side and which is relatively cheap to evaluate. This set is then solved iteratively using the linear terms as a kernel, and the nonlinear terms on the right-hand side are re-evaluated at each iteration using the most-recent values. The linear set can be algebraically reduced to the solution of a three-dimensional elliptic-boundary-value problem, the horizontal aspects of which are discussed in detail in Appendix B of Côté and Staniforth (1990). In practice the cost of solving the coupled set of nonlinear equations is only marginally more expensive than the iterative solution of the variable-coefficient linear set. The most significant contribution to the cost of a timestep is that of interpolation, which is the same regardless of whether the coupled set of equations is linear or nonlinear.

5. RESULTS

5.1 Methodology

A preliminary assessment of the above-described global variable-mesh strategy was made in Côté et al. (1995) by performing three 48-h integrations starting from the same initial data, the Canadian Meteorological Centre analysis valid at 12 UTC 12 Feb 1993. For all integrations, the model was run with 23 vertical levels (p_T = 10 hPa) using a 30-min timestep: a Laplacian diffusion was included with a

coefficient of 1.5×10^5 $m^2 s^{-1}$. There was no topography and there were no heat or momentum fluxes. The first two experiments were performed to assess the impact on the forecast of changing the orientation of a uniform-resolution (1.2°) mesh by 39° along a meridian. It was found that the global rms differences between the two 48-h forecasts are acceptably small: 4.9 m for the 500 hPa height field (which is about 5.5 km above the Earth's surface), and 0.6 hPa for the mean sea-level pressure (mslp), which amounts to less than one part in a thousand. The second and third experiments were performed to verify the thesis that the 48-h forecast over a 81.6° x 60° uniform-resolution (1.2°) window centered at (103°W, 51°N) over N. America can be well reproduced at a fraction of the cost of using 1.2° uniform resolution everywhere. Note that the points of the two meshes were coincident over the uniform-resolution window. Over this window the rms 500 hPa height and mslp differences of the two forecasts were respectively found to be 7.0 m and 0.6 hPa.

It was also mentioned that it would ideally have been preferable to run these experiments at the same 0.5° resolution as for the analogous ones presented in Côté et al. (1993) for the shallow-water (2-d) prototype, but it was not possible to do so at that time since computer-memory management had not yet been sufficiently optimized. Although this is still the case, it is nevertheless possible to increase the resolution by 50%. So in the present paper the experiments of the last of the two above-mentioned comparisons have been redone, but with the resolution increased from 1.2° to 0.8°, and the timestep reduced from 30 mins to 20 mins, all other parameters remaining unchanged.

The mesh configurations (only every third latitude and longitude are shown for pictorial clarity) of the two experiments are displayed in Figs. 6 a-b, and their attributes are summarized in Table 1. Expt A is run with *uniform* resolution, whereas Expt B is run with *variable* resolution. The mesh of Expt B is coincident with that of Expt A over its 81.6° x 60° uniform-resolution subdomain: it has 5.25 fewer degrees of freedom. The resolution of the variable mesh of Expt B degrades smoothly away in each direction (each successive meshlength is approximately 10% larger than its predecessor) from the 81.6° x 60° uniform-resolution (0.8°) window centered on a point of the equator of the rotated coordinate system. This point is located at (103°W, 51°N) in geographical coordinates as in the analogous experiments of Côté et al. (1995). Uniform resolution again refers to uniform spacing in latitude and longitude: however the meshpoints of the window are also almost uniformly spaced over the sphere with a meshlength that varies between approximately 76 and 88 km.

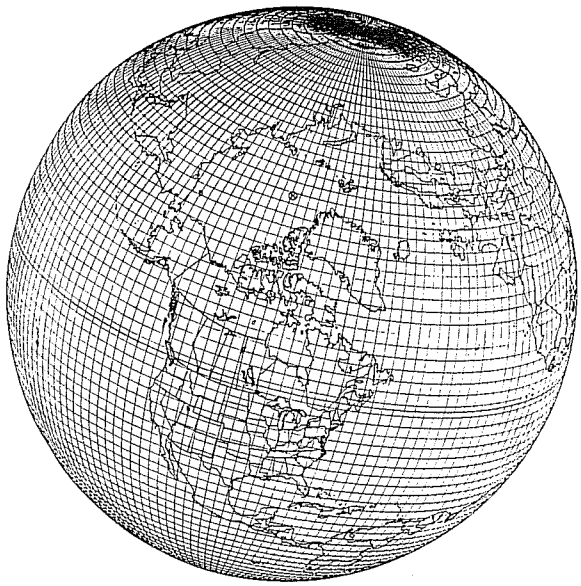

Fig. 6(a) The uniform 0.8° resolution 450 x 226 mesh used for Expt A: for clarity only every 3rd point in each direction is plotted.

Fig.6(b) A variable-resolution 162 x 120 mesh having an 81.6° x 60° window of uniform 0.8° resolution, centered on (103°W, 51°N), and used for Expt B: for clarity only every 3rd point in each direction is plotted.

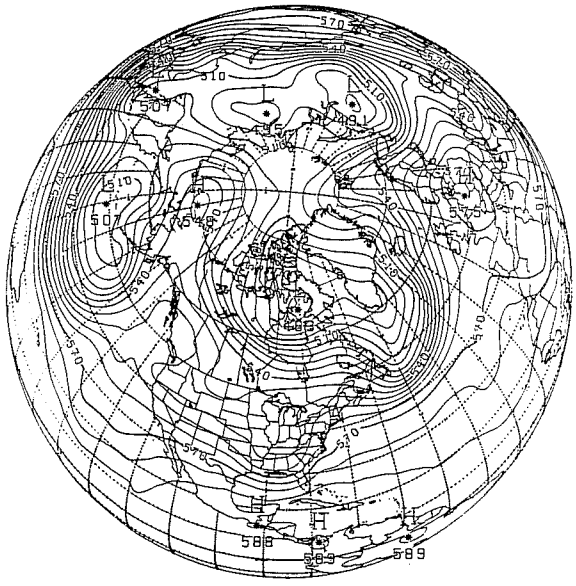

Fig. 7 Initial geopotential height at 500 hPa in dam on an orthographic projection; contour interval = 6 dam.

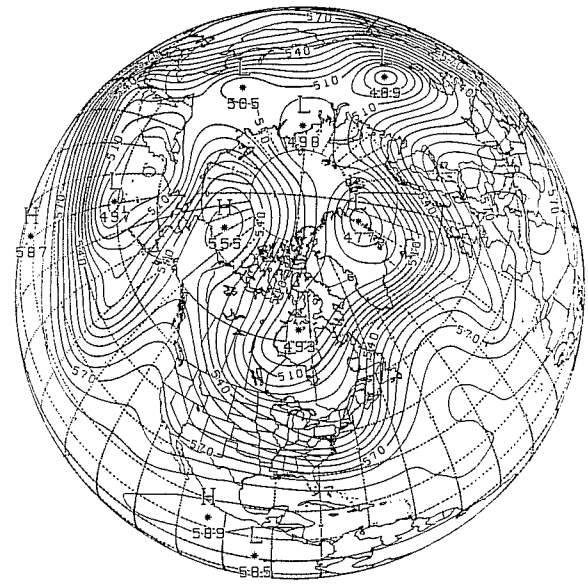

Fig. 8 Same as in Fig. 7, but at 48-h for Expt A.

Expt	Rotated Coordinate System?	Mesh: Uniform/ Variable	Dimensions	Resolution
A	Yes, centered on (103°W,51°N)	Uniform	450 x 226	0.8° everywhere
B	Yes, centered on (103°W,51°N)	Variable	162 x 120	0.8° on 81.6° x 60° window

Table 1: Experimental configurations.

5.2 The experiments

The 500-hPa height field of the initial analysis used for the experiments is shown in Fig. 7. The integration of Expt A (i.e. uniform resolution everywhere in the rotated coordinate system) is considered to be the ground truth for the purposes of validating the 48h forecast of the variable-resolution integration (Expt B): the meshes of both integrations are identical over the uniform-resolution window of Fig. 6b. The 2-day variable-resolution forecast is shown in Fig. 9 and may be compared to that of the control (Fig. 8). The two forecasts (Expts A vs B) are quite close over the uniform-resolution area of interest (defined by the curvilinear rectangle of Fig. 9). This confirms the thesis that the forecast over the 0.8° uniform-resolution window can be well reproduced at a fraction (about a fifth) of the cost of using 0.8° uniform resolution everywhere. However they are significantly different over areas of low resolution, as indeed they are expected to be. Quantifying this, the global rms differences between the forecasts of Expts A and B are respectively 26.6 (26.8) m and 3.3 (3.4) hPa for the 500 hPa height and mslp fields, where the corresponding Côté et al. 1995 results are given in parentheses. However over the curvilinear rectangle, where the meshpoints of the two grids are coincident, they are only 6.1 (7.0) m and 0.6 (0.6) hPa.

Note that the spatial truncation errors associated with the variable-resolution portion of the model's grid propagate with the speed of the local wind. This has to be taken into account when defining a uniform-resolution region of interest for the model. It has to be sufficiently large, so that the entire region is not unduly contaminated by the error advected in from the variable-resolution portion of the grid during the time of integration. It is therefore a compromise between the width of this region and the length of the run. The differences between the forecasts of Expts A and B increase as a function of the proximity to the upstream boundaries of the uniform-resolution window, due to the inflow from the coarser-resolution outer domain (see Fig. 10). In principle they should be somewhat smaller if the experiments were to be run at 0.5° resolution instead of 0.8°, since the inwardly-propagating upstream flow of Expt B would then be better resolved. However it is important to realise that the initial conditions of the two experiments are deficient in the sense that they are not in good dynamic balance.

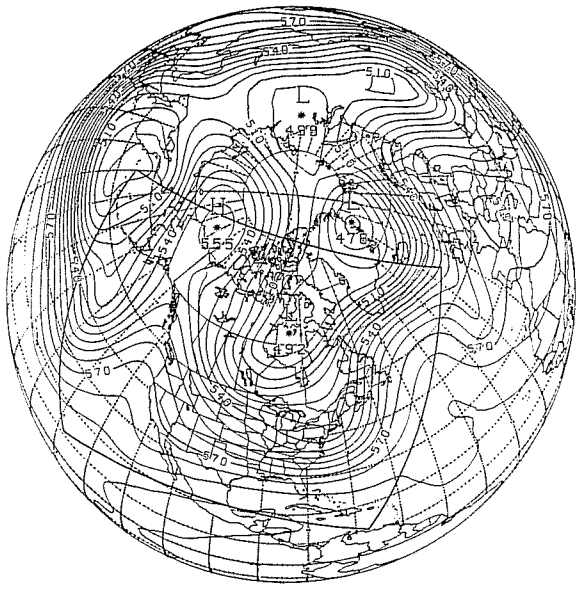

Fig. 9 Same as in Fig. 7, but at 48-h for Expt B.

Fig. 10(a) Difference between 48-h forecasts of Expt A and Expt B for 500 hPa geopotential height; contour interval = 6 m.

Fig. 10(b) Same as (a) but for mslp ; contour interval = 2 hPa.

The analyses are consistent with an underlying orography, which has been "removed" in the present experiments for a simplified atmosphere. Consequently some large-scale gravity waves of unrealistically-large amplitude are created: they subsequently propagate, and slosh about during the integration, and they do so with different phase speeds. Evidence of this can be seen in the time traces (not shown) for the surface pressure at a point in the uniform-resolution subdomain located at (100°W, 48.2°N), and the amplitude of the surface pressure oscillation is a couple of hPa or so. With dynamically-balanced initial conditions (e.g. obtained using a digital filter) the time traces would presumably be significantly smoother, and the differences between the two integrations consequently reduced.

6. SUMMARY AND CONCLUSIONS

The 1-parameter family of $O(\Delta t^2)$-accurate schemes introduced in RSR94 to address the problem of the spurious resonance of semi-implicit semi-Lagrangian schemes at large Courant number, has been generalized to a two-parameter three-time-level family by introducing the possibility of evaluating total derivatives using an additional time level of information. The RSR94 family can be considered to be the limiting case of the generalized family that maximally simplifies the evaluation (using a two-time-level difference) of the total derivatives. The other limiting case is the "backward-implicit" scheme, where maximum simplification of the evaluation (entirely at the arrival point) of the other terms occurs, and where an additional (third) time level is employed to evaluate the total derivatives. It has the virtues that the only upstream evaluations required are those associated with the total derivatives, and that it does not require derivative terms such as $\nabla\phi$ and $\nabla \cdot V$ to be evaluated at any time other than the present one (which is done implicitly and only at arrival meshpoints). Both of these limiting cases are off-centered discretizations, to avoid spurious resonance, and all schemes examined are $O(\Delta t^2)$ accurate.

Resonance, stability and truncation-error analyses have been performed for the proposed generalized family of schemes. Theory then leads to the following conclusions:

a) to avoid instability and resonance the domain of validity for the parameters is ($\delta > 0$, $\varepsilon > -1/2$);

b) it is advisable to choose δ and ε from the more restricted domain ($\delta > 0$, $\varepsilon \geq 0$), to avoid having a time-decoupled computational Rossby mode;

c) it is also advisable to use the smallest-possible values of δ and ε (consistent with being adequately off resonance), to respectively minimize the truncation errors and to maximally damp the computational Rossby mode;

d) the backward-implicit scheme has twice the damping rate of the RSR94 scheme, even though they both have the same leading-order truncation error;

e) although there is a sub-family of the generalized family of schemes that is formally $O(\Delta t^3)$-accurate ($\delta = -1/6$, ε free), it is unstable for the gravity modes; this is unfortunate; starting from a stable-but-resonant centered two-time-level scheme ($\delta = \varepsilon = 0$), a degree of freedom can be added to address resonance (by using an additional time level and thereby decentering either the evaluation of the total derivatives or the other terms), but adding a further degree of freedom (while still only using three time levels) does not permit increasing accuracy to $O(\Delta t^3)$; and

f) a corollary of e) is that the $O(\Delta t^3)$-accurate scheme tentatively proposed in McDonald (1987) is unstable for gravity modes.

Sample integrations for various members of the generalized family were performed using a shallow-water model. It was found that the results were consistent with the theory, and that stable non-resonant forecasts at large Courant number are possible for a range of values for the δ and ε parameters. Within the RSR94 family of schemes, the scheme ($\delta = 1/2$) for which results were shown in RSR94 is a good choice but not an optimal one. A smaller value of δ than 1/2, but no smaller than 1/6, can reduce the leading-order term for the truncation error by as much as a factor of 2 (see 2.32) and the damping rate by as much as a factor of 3 (see 2.33), while still acceptably controlling resonance. It was found that while either of the two methods presented in RSR94 for computing the trajectories is acceptable for their scheme, only one of them is acceptable at large timestep for some members of the generalized family. The method that computes the trajectory in a piecewise fashion is therefore to be preferred to the one that uses a single great-circle trajectory.

A two-dimensional 'proof-of-concept' prototype of a variable-resolution global model has been available for some time now. It has been found that the overhead associated with using a model of global extent for short-range forecasting, even at the scale of several kilometers, is relatively small: more than half of the total number of meshpoints are over the uniform-resolution area of interest, and the overhead of using variable resolution outside this area is consequently comparable to that of the sponge regions of driven limited-area models. The generalization of the formulation to three space dimensions is outlined in the present paper and some preliminary results with an adiabatic version of this baroclinic model are presented. They confirm the potential of the proposed strategy: differences between the 48-h forecasts for the 500 hPa geopotential height and mean-sea-level pressure fields obtained from a uniform 0.8° model, and those obtained from a variable-mesh model with equivalent resolution on a 81.6° x 60° sub-domain, are acceptably small.

REFERENCES

Bates, J R, S Moorthi, and R W Higgins, 1993: A global multilevel atmospheric model using a vector semi-Lagrangian finite-difference scheme. Part I: Adiabatic formulation. *Mon. Wea. Rev.*, **121**, 244-263.

Coiffier, J, P Chapelet, and N Marie, 1987: Study of various quasi-Lagrangian techniques for numerical models. Proceedings of ECMWF Workshop on Techniques for Horizontal Discretization in Numerical Weather Prediction Models, 19-46, European Centre for Medium-range Weather Forecasts, Shinfield Park, Reading, U.K., 377 pp.

Côté, J, and A Staniforth, 1990: An accurate and efficient finite-element global model of the shallow-water equations. *Mon. Wea. Rev.*, **118**, 2707-2717.

Côté, J, M Roch, A Staniforth, and L Fillion, 1993: A variable-resolution semi-Lagrangian finite-element global model of the shallow-water equations. *Mon. Wea. Rev.*, **121**, 231-243.

Côté, J, S Gravel, A Méthot, A Patoine, M Roch, and A Staniforth, 1995: Preliminary results from a dry global variable-resolution PE model. *Atmosphere-Ocean*, André J. Robert Memorial Symposium issue, to appear.

Gravel, S, A Staniforth, and J Côté, 1993: A stability analysis of a family of baroclinic semi-Lagrangian forecast models. *Mon. Wea. Rev.*, **121**, 815-824.

Héreil, P, and R Laprise, 1995: Sensitivity of internal gravity wave solutions to the timestep of a semi-implicit semi-Lagrangian nonhydrostatic model Manuscript submitted to *Mon. Wea. Rev.* and available from R Laprise, Dept of Physics, Université du Québec à Montréal, P.O. Box 8888, Stn. A, Montréal, P.Q., Canada, H3C 3P8.

Kaas, E, 1987: The construction of and tests with a multi-level, semi-Lagrangian and semi-implicit limited area model. Diploma thesis, Geophysics Institute, Copenhagen University, Copenhagen, Denmark, 117 pp.

McDonald, A, 1987: Accuracy of multiply-upstream semi-Lagrangian advective schemes II. *Mon. Wea. Rev.*, **115**, 1446-1450.

McDonald, A, and J E Haugen, 1992: A two-time-level, three-dimensional semi-Lagrangian, semi-implicit, limited-area gridpoint model of the primitive equations. *Mon. Wea. Rev.*, **120**, 2603-2621.

Purser, R J, and L M Leslie, 1994: An efficient semi-Lagrangian scheme using third-order semi-implicit time integration and forward trajectories. *Mon. Wea. Rev.*, **122**, 745-756.

Ritchie, H, and C Beaudoin, 1994: Approximations and sensitivity experiments with a baroclinic semi-Lagrangian spectral model. *Mon. Wea. Rev.*, **122**, 2391-2399.

Ritchie, H, C Temperton, A Simmons, M Hortal, T Davies, D Dent, and M Hamrud, 1995: Implementation of the semi-Lagrangian method in a high-resolution version of the ECMWF forecast model. *Mon. Wea. Rev.*, **123**, 489-514.

Rivest, C, A Staniforth, and A Robert, 1994: Spurious resonant response of semi-Lagrangian discretizations to orographic forcing: Diagnosis and solution. *Mon. Wea. Rev.*, **122**, 366-376.

Rivest, C, and A Staniforth, 1995: Modifying the conventional three-time-level semi-implicit semi-Lagrangian scheme to eliminate orographically-induced spurious resonance. *Atmos.-Ocean*, **33**, 109-119.

Robert, A, T L Yee, and H Ritchie, 1985: A semi-Lagrangian and semi-implicit numerical integration scheme for multilevel atmospheric models. *Mon. Wea. Rev.*, **113**, 388-394.

Staniforth, A, and J Côté, 1991: Semi-Lagrangian integration schemes for atmospheric models - a review. *Mon. Wea. Rev.*, **119**, 2206-2223.

Tanguay, M, A Simard, and A Staniforth, 1989: A three-dimensional semi-Lagrangian scheme for the Canadian regional finite-element forecast model. *Mon. Wea. Rev.*, **117**, 1861-1871.

Tanguay, M, A Robert, and R Laprise, 1990: A semi-implicit semi-Lagrangian fully compressible regional forecast model. *Mon. Wea. Rev.*, **118**, 1970-1980.

Tanguay, M, E Yakimiw, H Ritchie, and A Robert, 1992: Advantages of spatial averaging in semi-implicit semi-Lagrangian schemes. *Mon. Wea. Rev.*, **120**, 124-130.

Williamson, D L, and J G Olson, 1994: Climate simulations with a semi-Lagrangian version of the NCAR CCM2. *Mon. Wea. Rev.*, **122**, 1594-1610.